Society of Photo-Optical Instrumentation
Engineers, Instrumentation in Astronomy III
Symposium, Tucson, Arizona, Jan. 29 to
Feb. 1, 1979

POSITION SENSORS AND ACTUATORS FOR FIGURE CONTROL OF A SEGMENTED MIRROR TELESCOPE

George Gabor

January 1979

Prepared for the U. S. Department of Energy
under Contract W-7405-ENG-48

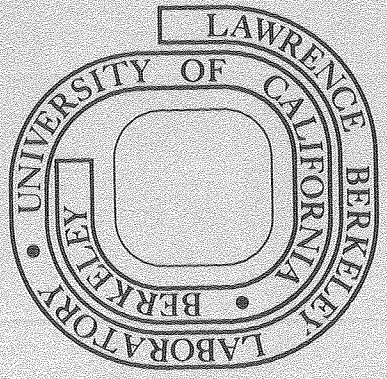

DISCLAIMER

Position Sensors and Actuators For Figure Control of a Segmented Mirror Telescope

George Gabor
Lawrence Berkeley Laboratory, University of California
Berkeley, California 94720 U.S.A.

Abstract

A control system using mirror displacement sensors and position actuators to maintain proper surface control of a segmented mirror is summarized. The system is composed of three major components; a figure control computer, displacement sensors and displacement actuators. Desired positioning accuracy is 50 nm. Several methods for achieving the needed sensor sensitivity and stability are discussed. A capacitive bridge detector was chosen and its expected and measured behavior is described. Two mechanisms for positioning a mirror segment to optical tolerances, yet having a large dynamic range to compensate for mirror cell deformation are reviewed. Test results for a roller screw are given with an outline of the servo loop design.

Introduction

The University of California has initiated a design study for a large optical telescope.[1] As part of the study two types of primary mirror design are being explored, one of which is segmented. This paper will discuss the preliminary designs and initial test results of two critical components for controlling the figure of a segmented telescope mirror; mirror position detectors and mirror position actuators. The advantages of a segmented primary mirror have been outlined elsewhere.[2] These include light weight, low cost, low risk of catastrophic failure, and reduced fabrication time. Paramount for the achievement of a segmented optical surface is a method for measuring the positions of the mirror surfaces and a way to position the mirrors to optical tolerances. Both these functions must be performed reliably and with low maintenance under a large range of environmental conditions.

A general description of the telescope, the segmented mirror design, and figure control algorithm were given in the previous paper.[2] The geometry chosen for the 10 meter diameter segmented primary mirror is a hexagonal pack of 54 - 1.4 meter diameter mirrors, 10 centimeters thick, around a 3.5 meter diameter central fixed reference mirror. Each segment is held from the back by nine support points attached in groups of three to three whiffle trees. Each whiffle tree is attached to an actuator. A total of 162 actuators are required. The displacement sensors will be mounted on the back of each mirror segment at the interface edges, bridging across to the adjacent mirror. Each hexagonal face will have two sensors, one near each vertex, for a total of 288.

Because of the interlocking nature of the hexagonal design, measurement of adjacent mirror displacements suffice to define both axial displacements and, through the moment arm between detectors, the tilt of the segments. Thus, the position sensor need only measure displacements normal to the mirror surface, and should be insensitive to motion in other directions. From the optical resolution requirements and control algorithm,[3] it is found that the individual position detectors should have 50 nm rms resolution. The actuators should have a comparable positioning resolution of 50 nm. The detectors and actuators will both have to accommodate the gravitational and thermal deformations of the mirror support structure, expected to be about 2-3 mm.

Since the proposed telescope is to be used both for visible as well as infrared work, a high elevation dry site is necessary. Observing will be done both day and night. These operating conditions set the environmental requirements as follows: barometric $\Delta P = 0.1$ atmosphere; operational wind velocity 50 mph; temperature range -30°C to +25°C; humidity 0-100%. The installation will have to be dust and insect proof and immune to normal electrical noise and resist the effects of lightning. Maintenance should be easy, i.e. modular.

The bandwidth of the control system will be limited by the natural resonance of the mirror support structure (expected to be approx. 10 Hz). The effects of wind loading on the support structure are not known in detail, and will depend on the as yet undefined extent and position of the slit in the dome. Since the energy content of the wind at frequencies above 10 Hz is expected to be rather small, barring any dome resonant effects, the effects of wind should be greatly reduced by the control system.

Control System

The mirror control computer (MCC) optimizes the mirror figure by using displacement detector readings in a least squares fitting algorithm to calculate the present actuator locations. The MCC then calculates and transmits actuator correction values which will move the segments so the displacement detector readings will match the values previously determined for each detector during calibration. After the actuators have moved, new detector readings are taken and the optimizing cycle repeats. This procedure continues at a $\approx$10 Hz rate. The calibration procedure finds the set of detector readings which give the best image resolution. This is done by superimposing the focal points of the segments on that of the central mirror.

As shown in Figure 1, the MCC receives over a bidirectional buss displacement detector outputs and actuator locations. Each segment's bidirectional multiplexer is fed control information by the MCC and a master oscillator signal. A master clock is required to synchronize the detector oscillators thereby avoiding any heterodyne problems in the 288 detectors. The multiplexer talks bidirectionally to both the six position detectors and the three actuators. Digitizing of the analog displacement signals from the position detectors is done at each segment node.

Maintaining the mirror figure requires that the displacement detector be an extremely stable measurement device; the noise level must be under 50 nm and the allowed drift under 10 nm per week in its normal operating mode. The calibration procedure requires that the detector be predictable to 1 part in 800 over $\pm$ 20 micron displacements. An actuator transmits its location and receives position changes. A local servo loop maintains the mechanical position of the actuator at a location assigned by the MCC.

Displacement Actuator

Design Criteria

The displacement actuator must operate in the environment outlined above and perform displacement operations at least as small as 50 nm. It must operate smoothly at this level as well; that is it must at least behave monotonically at this level. An actuator must support the weight of the mirror--a load of about 120 kg, plus a preload to 50 kg. To minimize power losses to the environment, the overall efficiency should be high, at least 85%, and the resonant frequency should also be high, above a few hundred Hertz. Displacements of $\pm$ 2 mm with $\leq$ 25 nm resolution and slewing rates of about 3 mm/min are desirable. The device should also have (with annual maintenance) an expected lifetime of approx. 40 years and should be inexpensive and easy to fabricate and maintain.

The amount of heat generated by the actuators and any other components in the back of the mirror must be kept to a minimum, both to minimize the heating effects on the mirrors and to reduce the thermal turbulence and resulting bad "seeing" in the dome. Consequently the actuator's power usage must be kept low during operation, particularly when simply sitting at a fixed position. External cooling of major heat dissipating components is possible but undesireable.

The actuator package should also be able to store the location supplied by the MCC, calculate and supply drive signals to the torque motor, monitor the actuator behavior and send the appropriate housekeeping and safety information to the MCC.

Actuator Displacement Mechanism

A variety of different types of displacement devices were considered including hydraulic, pneumatic, piezoelectric, peristaltic, lever, screw, and combination actuators. The devices which seemed to hold the most promise of meeting the above requirements are differential ball screws and roller screws.

The principle of operation of a differential ball screw is as follows. Two opposite handed screws are made on a common shaft with slightly different pitches. When the shaft rotates, the nuts on the two different pitches will move relative to each other at a rate set by the difference of their respective pitches. Thread contact is made with roller balls, thereby reducing friction by at least a factor of 100 over the sliding friction of a standard nut. These screws have the disadvantage that the load carrying capacity is reduced, since the load is carried on the point contact of the balls. Successful differential ball screws actuators in tilting mounts have been manufactured by Rocketdyne Division of Rockwell for laser mirrors at Los Alamos Scientific Laboratory.

Precision roller screws are a recent addition to the bearing screw family. Figure 2 shows the contruction of a recirculating planetary roller screw. Unlike the differential ball screw the roller screw nut advances one pitch length per screw revolution. The planetary rollers are reset by the differentials at the ends of the nut. As the nut turns, each roller is sequentially lifted and reset one pitch length backwards. By using rollers in the nut, a line contact is made with the screw which gives the roller screw its large load carrying capacity. A 12 mm diameterscrew with 1 mm pitch can carry 540 kg for a life of 2.5 x 10^6 cm travel.

Actuator Design

A displacement actuator using a roller screw is being designed and built. Figure 3 shows an electrical block diagram of the system. A microprocessor provides drive signals through a digital-to-analog converter to a class D amplifier that powers the torque motor. A 16 bit absolute shaft encoder feeds the location of the screw to the microprocessor and the segment node. A 1 mm pitch roller screw has been selected, and with a 16 bit encoder provides a minimum incremental resolution of 15 nm. The microprocessor uses the encoder address and its time derivatives with a local servo algorithm to calculate appropriate corrective drive signals. This algorithm accounts for non-coulombic friction behavior.[4,5] Excitation of mechanical resonances of the mirror support cell will be avoided by prohibiting synchronized unidirectional motion of all actuators. The mirror cell design has not yet been completed, but the expected primary resonant frequency is between 10 and 20 Hz. The brake is not used during normal operation of the telescope. The local feedback loop maintains the actuator's position by suppling a correction pulse, independent of the MCC

update rate, to the torque motor if the encoder address is different than the stored address. Mechanical limit switches and the servo program protect the actuator from over driving by cutting off torque drive and engaging the brake.

The mechanical layout of the actuator is shown in Figure 4. The unit is hermetically sealed at one end by a rubber diaphram and an O-ring at the other. The power and control cables exit through seals in the hollow pivot shaft. The limit switches are easily adjusted in their forward location. A preloaded linear roller bearing takes up screw reaction torque and the radial mirror load. The back of the actuator rod encases the roller nut and is hollowed to accept the screw. The brake is placed in between the roller screw nut and torque motor to reduce the moment of inertial and acceleration-dependent error between the torque motor and shaft encoder. The thrust bearing is just behind the torque motor to minimize any wind-up in the screw. If the screw were rigidly held, the twist produced by the maximum torque available from the motor is 0.6 arc seconds per cm of screw length. Therefore, the shaft encoder will faithfully follow the torque motor motion.

Roller Screw Test

A critical component in the actuator design is the roller screw. Consequently a precision roller screw with a 12 mm diameter and 1 mm pitch was obtained for test and evaluation.[6] A fixture was fabricated to test its smoothness, monotonicity, hysteresis and slipstick. The fixture (Figure 5) consists of an interferometer illuminated by a spherical wave front from a He-Ne laser (λ = 632.8 nm), which produces a Newton ring interference pattern. A narrow field of view phototransistor detector measures the intensity variations of the interference pattern as the screw is rotated. The displacement resolution is better than $\lambda/50$. The target mirror is hinged so that it is both displaced and tilted as the screw advances. A steel ball mounted on the end of the screw pushes against a glass flat on the back of the mirror. The tilt only has the minor effect of compressing the periodicity of the recorded fringe pattern by about 20% for the two degrees that the screw is able to turn. The nut is lightly retained radially with a thrust plate to take up the axial load. Two screws go from the thrust plate to a flat spring which provides 75 kg axial load to the roller screw through a thrust roller bearing. Just in front of the rear bearing, a 30 cm lever arm is clamped to the screw. A glass bearing surface is mounted on the end of the lever arm where a micrometer with a steel ball on its tip pushes against it. This provides a displacement reduction of 2000, so for example 20 µm micrometer displacements advance the roller screw by 10 nm. A reversible synchronous gear motor drives a flexible shaft attached to the micrometer spindle. The whole fixture is encased in a styrofoam box with exit ports for the micrometer and the interference pattern. The motor sits on top of the box on two layers of blister packing.

The initial tests were done with the roller screw just as it came from the factory. The first test was for smoothness. Multiple passes were made over each 2° of rotation for 30° (the limit of the fixture's adjustment). The motor drove the micrometer at 30 Rev/min or equivalent to a screw motion of 15 λ/min, first one direction then in reverse. A smooth sine wave was produced in both directions which indicates the screws has no roughness greater than $\lambda/20$ and is monotonic to that level. To test for backlash and slipstick, the screw was driven forward, stopped, then reversed at 1 λ/min. Backlash was less $\lambda/40$ with slipstick of about 20-30 nanometers.

The same tests were repeated after the roller screw was degreased, and lubricated with a constant-viscosity high-film-strength synthetic motor oil. Figure 6a shows the motion to be smooth and monotonic to better than $\lambda/20$. Backlash and slipstick have also been reduced to $< \lambda/40$ and are indicated in Fig. 6b.

An additional test was made by manually applying a step function of fixed baseline and varying amplitude in steps of 25 µm to the micrometer. The screw was set so a bright fringe was on the photo-detector. The results are presented in Figure 7 and show the screw displacement can be repeatably set to much better than 12 nm. Seismic noise equivalent to 5 nm displacement peak to peak is due to the pendulum the target mirror makes with the hinge.

The excellent results of these tests, even though it is a single sample, indicate that this type of roller screw will work in an actuator system.

In the future the entire actuator assembly will be tested for the same parameters as was the roller screw. In addition, a life test will be performed under maximum expected load and displacement travel. The life of the screw varies as the cube of the applied load and for our load the expected life is 2×10^8 cm travel. With high-frequency displacements in the micron range and low-frequency motions of 4 mm on a hour time scale the screw life should exceed that of the telescope.

Displacement Detector

Design Criteria

Our detector must operate in the previously defined environment and measure one direction of displacement with stability and accuracy better than 50 nm. Small orthogonal motions ≤ 1 mm should not substantially disturb the measurement. The detector must also operate with the same precision and stability over a

dynamic range of ± 20 μm, the range needed for the calibration procedures. Since the measurements will be made on the back of the mirror, it is critical that the back side accurately reflects the front surface position. To insure this, the expansion characteristics of the mirror material and the effects expansion has on the segments must be well understood.

Precision measurements of the thermal expansion coefficient (α) versus temperature were made by Berthold and Jacobs[7] for several low expansion materials. Table 1 is derived from their data.

TABLE 1

	α FOR GIVEN α = 0 TEMP.		$\frac{\delta\alpha}{\delta\Delta T}$	α = 0 TEMPERATURE IN °C
	@ -30°C	@ +25°C		
CER-VIT[1)]	6×10^{-8}	-9×10^{-8}	-2.7×10^{-9}	-10
ULE[2)]	-12×10^{-8}	-1×10^{-8}	$+2.0 \times 10^{-9}$	30
ZERODUR[3)]	13×10^{-8}	3×10^{-8}	-1.8×10^{-9}	40

Manufactured by: 1) Owens Illinois†, 2) Corning† and 3) Heraeus-Schott†

Over the temperature range of interest -30°C to +25°C, the materials listed in Table 1 have α's < 14×10^{-8}/°C. The α values of these materials vary approximately linearly with temperature in this temperature range. For a given type of material although α at a given temperature may vary for different samples, the rate of change of α with temperature ($\delta\alpha/\delta\Delta T$) is constant. As shown in Table 1, the value of α for the different materials goes to zero in or near the desired temperature span. The expansion characteristics of an individual piece of material for this specific temperature range, can be specified by simply stating the temperature at which α crosses zero. The expansion behavior, $\Delta L/L \propto T^2$, of the different materials between -30°C to +40°C are shown in Figure 8. Ideally, for minimum total expansion, the α equal zero point should fall at the mean value of the desired temperature range. With this characterization of these low expansion materials we will discuss two extreme situations.

The first case is if all the mirror segments have identical α's at a given temperature. To keep induced relative thickness variations to $\leq$ 50 nm, an acceptable value, the ajoining segment temperatures cannot differ by > 5°C. Normally such radial temperature gradients will not be encountered except if sunlight strikes a segment. The other case is if the segments are all at the same temperature, in the range of -30°C to +25°C, the relative thickness variations will be $\leq$ 50 nm if the range of α = 0 crossing point temperature is < 4°C. The ability of glass manufacturers to hold the α = 0 crossing point spread down to this level is not known at this time. If it proves impossible, one must resort to thermal calibration of the mirror segments.

Detector Design

Optical, inductive and capacitive techniques were explored for methods of sensing.[8-10] The requirements for long term stability, sensitivity of 50 nm rms under severe environmental conditions, large dynamic range, and ease of contruction and maintainence lead to the choice of capacitive sensing.

The use of capacitance change to measure small displacements started around the turn of the century and since then has been used in a variety of ways.[11-15] Its use in geophysical instruments is where the "state of the art" work has been done recently. Sensitivities of 10^{-14}m (T=1 sec) and 10^{-12}m drift per day[16] are achievable in a self-contained detector with a temperature controlled (ΔT = 0.001°C) atmosphere of helium at 10 mm of mercury pressure and a capacitor spacing of 25 micrometers. Though the telescope mirror displacement sensors only require 10^{-8}m sensitivity and drift per week, they will have to operate in a very severe environment with a capacitor spacing of 2 mm. The symmetry, both mechanical and electrical, of a capacitive bridge, led to its choice for the sensor configuration. By balancing two capacitors against one another, effects of temperature, barometric change, humidity and aging are reduced by at least several orders of magnitude. Several capacitive sensors were devised for mounting on the edge of mirror segments as well as on their backs. A back mounting detector was selected for its ease of maintainence and high level of isolation.

† References to a company or product name does not imply approval or recommendation of the product by the University of California or the U. S. Department Of Energy to the exclusion of others that may be suitable.

The detector can be broken up into two parts; the mechanical sensor, and the electronics. An electrical block diagram of the displacement detector is shown in Figure 9. The capacitive displacement sensor generates an error signal which is amplified, phase detected, and filtered, then transmitted to the segment multiplexer. The master clock signal, plus the setting of sensitivity and nulling are externally supplied by the MCC. The contribution of the electronics to detector performance will be discussed later in this paper. The basic stability of the system is limited by the interaction of the capacitive sensor and the environmental extremes.

A Capacitive Bridge Sensor

The capacitance between two plates, neglecting edge effects, is given by:

$$C = \frac{eA}{D} \tag{1}$$

Where e = dielectric constant
A = area of plates
D = separation of plates

For the bridge shown in Figure 10a, the change in capacitance for a small displacement is given by:

$$\Delta C = C_2 - C_1 = \frac{eA}{X_0} \cdot \frac{2X}{X_0} \cdot \frac{1}{1 - \frac{X}{X_0}^2} \tag{2}$$

But $eA/X_0 = C_0 = C_1 = C_2$ when the center plate is equally spaced between two outer plates. The equation shows for this configuration we get twice the capacitance change for a given displacement and that the change is linear to 0.01% for 1% changes in X/X_0. Edge effects are eliminated by the use of the circuit of Figure 10b and a ground ring around each of the sensing plates P1 and P2. The driving plate, P3, extends well beyond P1 and P2. The circuit incorporates a charge sensitive amplifier which responds to any charge input from the sensor by changing its output voltage such that:

$$V_0 C_F = V \sin \omega t \, \Delta C \tag{3}$$

where C_F is the feedback capacitance. Because of the high open loop gain (10^6) of the preamp, the sensor plates P1 and P2 are held at virtual ground. The grounded ring around the edges of P1 and P2 suppresses any field from extending off the edges of the plates, thereby effectively eliminating edge capacitance. Figure 11 shows the arrangement of the test sensor and how the ground ring extends completely around the sensor plates avoiding edge effects and any stray noise pickup. The further advantage of maintaining the sensor plates at virtual ground is that a small change in C_S, the stray capacitance to ground, has no effect on detecting the displacement signal as long as the preamp has a large loop gain.

A change in the dielectric constant of the space between the plates, from Eq. (2), will change the displacement signal V_0, proportional to the dielectric change. If we put a protective boot around the sensor to exclude insects and dust, density variations of the air due to temperature and barometric changes and humidity changes will still effect the detector output when it is not mechanically centered. Using the dimensions of the test capacitive sensor and the 20 micrometer displacement requirement for the calibration procedure , we find a 55°C temperature change would produce a 1.7 nanometer error, a .05 atm barometric change, a 0.5 nanometer error; and a 0 to 100% humidity change @ 25°C, a 2.1 nanometer error. Rhodium plating of the metallic surfaces of the sensor will reduce the effects of any condensation by helping the wetting of the surface. The effect of water is the same, whether it is vapor, liquid or solid, as long as it is uniformly distributed.

Mechanical Design

The ultimate stability of the displacement detector hinges on the mechanical characteristics of the capacitive sensor. Some of the causes of unwanted motion are thermal expansion, creep with thermal cycling of the metallic coating and bulk material, vibration, geometric distortion of the transducer mounting, deformations from gravitational force changes as the mirror tilts, and sensitivity to radial motions of the segments.

A cross-section sketch of an "actual" sensor (Figure 12) shows the encasing dust boot and the constant force mounts, clamping the body and paddle to their respective mirrors. Cer-Vit C101 and a 5 micron layer of copper metallization were picked as the construction materials. Thermal effects due to expansion of the sensors are only half as much those for the mirror; i.e., 5°C differential for 25 nanometers displacement error. Joint creep with thermal cycling can be avoided if contact areas are of identical material. Long term creep or aging due to relaxing of stresses in the sensor materials is less than 0.1 nanometer per month[17] and its effects are removed by the periodic calibration. The metallic electrode coatings are applied symmetrically about each piece of the sensor (Figure 11) which reduces any stresses coating temperature changes might cause. The resonant frequency of the sensor is much higher than the required telescope band pass of 10 Hertz and does not couple energy into the band pass. By design, the mirror segment will distort only very slightly under the varying gravitational load, typically < 50 nm. The differential deflections at a sensor position will be far less. The varying direction of the gravitational force on the sensor paddle with changes of mirror elevation will cause noticeable paddle deflections. A paddle 2 cm thick, and 10 cm long will deflect about 50 nanometers at the sensor center moving from the vertical to the horizontal. Since this deflection is predictable, a lookup table versus elevation would remove its effects.

As noted above the control system is designed to control the segment motions giving rise to tilt and focus of the image. The image is relatively insensitive to motions of the segments in the plane of the mirror. These need only be constrained to less than 2 mm to maintain the surface coherency to $\lambda/10$. Assuming the mechanical support limits overall motion to this level, the differential motion between adjacent segments is expected to be less than 0.5 mm. Such radial motions of the capacitive sensor paddle if it were mechanically perfect, would give rise to 4 nm displacement signals. This effect could be eliminated using a spherically shaped paddle instead of a flat paddle. If the paddle is not mounted perpendicular to the mirror axis, radial motion will produce a displacement output. For the proposed sensor dimensions, this error amounts to 2.5 nm/$\sqrt{n}$. Fabrication errors will also make the sensor sensitive to radial motions. Errors in the thickness of the sensor will also give a signal of 2.5 nm/$\sqrt{n}$.

Sensor Electronics

The electronics controls the detector's performance in three parameters: maximum sensitivity, dynamic range, and drift due to stray capacitances, which has been previously discussed. Since this type of capacitor is electrically noiseless, the dominant input noise generators are the input field effect transistor and the feedback resistor in the preamp and any induced voltages due to the driving voltages.

The chosen sensor geometry has the displacement sensitivity of 7×10^{-12} farad/mm. If the drive voltage is 1 V rms, the preamp input noise is equivalent to 45 nV or a displacement noise of 0.07 nanometers for a 100 Hz bandwidth. The leakage from the drive signal cannot be held to the same level as the preamp noise, but it will be small, and by design, held at a stable level by fixing the cable geometry. This small amount can then be electrically nulled. The dynamic range of the detector is limited to 10^4 by the amplifier's maximum linear output amplitude (about 10 V) and the minimum signal that can be reliably transmitted (1 mV with a signal-to-noise ratio of 10:1). This fits the required range if 1 mV corresponds to 2 nm.

The Test Detector

A test detector was fabricated using the above considerations. The sensor is shown in Figure 11. It is constructed of copper plated Cer-Vit C101 pieces with a hole drilled through the center of each end piece so that the sensor plate signals can be brought out. Four holes were drilled in each plate for bolting the assembly together, Unplated Cer-Vit (2 mm thick) is used for the spacers. All the pieces were optically polished flat to 0.5 μm or better. The central piece is parallel to 5 microns. To improve the plating adherence the pieces were etched very lightly producing pits < 1 micron deep. The surfaces of the sensor were cleaned with USP absolute ethyl alcohol and assembled, blowing the spacers with dry nitrogen just before clamping the assembly together.

Coaxial cables (15 cm) bring out the signal from the sensor plates to a summing junction box. The driving signals are also brought to the center plane by coax from a junction box. The driving transformer is doubly shielded and contained in a Pomona box--as are the balance transformer and balancing potentiometer. A 10 Pf NPO capacitor couples the balance signal to the input of the preamp. A Tektronics constant amplitude oscillator set to 50 kHz is used for the driving signal. The oscillator proved to be stable to only 0.6% which increased the apparent noise level when the detector paddle was displaced for calibration. The amplifier and phase detector were in separate modules powered by a NIM bin. The preamplifier is a modified solid-state detector preamplifier. The amplifier is a nuclear spectroscopy gaussian shaping amplifier. The precision phase detector is a balanced bridge design similar to one by Grimbleby and Harding.[18] The bandwidth (200 Hz) of the system is set by the integration time of the phase detector.

Calibration and Test Results

The sensor was placed on edge in a vacuum chamber with the preamplifier, driver transformer and balance box just outside the chamber. The sensor was connected to the preamplifier and drive transformer through isolated vacuum tight connectors by 150 cm total length of cable in each leg.

A 25 micron shim was inserted on one side of the sensor to calibrate the displacement sensitivity before and after the tests. The sensitivity remained 320 μV/nm for the two week duration of the tests. There was a 1.1 micron equivalent offset signal before balancing. The noise level output of the electronics was less than 50 μV, equivalent to 0.16 nm with the sensor attached. The drift of the electronics was less than 100 μV during testing. No attempt was made to control the temperature which ranged between 15°C to 25°C during the tests. An environmental chamber is being obtained to do the temperature testing.

The first test compared the detector output using air and then vacuum as the gap dielectric. As predicted, no noticeable output change was observed. The stability of the detector was tested in air over a six day period. Figure 13 shows the results. A general long term drift is apparent with additional variations due to the varying room temperatures. The temperature varied from about 15°C on the weekend (when the thermostat was turned down) to about 25°C during the week with shorter period variations caused by heater cycling. The approximate 11 nm/week drift appears to be caused by the creep of the sensor sections due to their vertical position and the copper plating of each segment between each spacer surface. Further tests are being performed to determine the cause of the temperature sensitivity and drift.

Displacement Sensing Errors

We now summarize the major sources of expected error in the displacement detectors sensing of the location of the mirror surface:

Gravitational deformation of paddle	50 nm*
Variation in segment expansion coefficient	50 nm*
Temperature differences between segments (1°C)	10 nm*
Radial displacements of flat paddle (gravitational, thermal)	4 nm*
Atmospheric effects (pressure, humidity) with 20 μm offset	4 nm
Mechanical distortion	1 nm
Creep of glass due to aging	0.1 nm/month
Electronics	1 nm
Angular misalignment of the paddle (at 0.5 mm radial displacement)	2.5 nm*/$\sqrt{n}$
Misalignment of sensor plates due to fabrication tolerance at 0.5 mm radial displacement	2.5 nm*/$\sqrt{n}$

*removable by calibration or calculation

The majority of the displacement error sources behave in a predictable fashion either as a simple function of temperature or elevation of the mirror. Corrections to displacement detector readings will be performed by the MCC. The manufacturing and installation tolerance errors can be minimized by careful design and production.

Conclusion

This paper details the progress of the design and development of some components for controlling the figure of a segmented telescope mirror. The preliminary design criteria for the control, position sensing and positioning device have been detailed. Testing of the critical component in the actuator and a prototype displacement detector have yielded very positive results. Detailed work still needs to be done on different aspects of the design. But the findings to date make me very optimistic, that the segmented mirror control system described above can be fabricated and work to the design specifications.

Acknowledgements

A special thanks to Jerry Nelson for many hours of helpful discussions defining problems and increasing my knowledge of telescopes and astronomers. My great appreciation to the many mechanical and electronic technicians who helped fabricate the hardware, especially to the people in my group; Reid Brandon, Dan Meier and Mike Strathman. I wish to express my appreciation to the Director of the Laboratory, Dr. A. Sessler for the support and funding of this project. Also, Thanks go to my wife Audrey for her secretarial help and lost weekends.

This work was performed under the auspices of the Division of Basic Energy Sciences of the U. S. Department Of Energy under Contract W-7405-ENG-48.

References

1. Nelson, J., Optical Telescopes of the Future, ESO Conference Proceedings, pp. 133-141, Dec. 1977
2. Nelson, J., "Segmented Mirror Design for a 10 meter Telescope", SPIE Proceedings, Vol. 172, Instrumentation in Astronomy III, Tucson, Az., Jan. 29 to Feb. 1, 1979.
3. Mast, T. S. and Nelson, J., "Figure Control of a Segmented Telescope", Lawrence Berkeley Laboratory report, LBL-8621. 1978.
4. Dahl, P.R., "Solid Friction Damping of Mechanical Vibrations", AIAA Journal, Vol. 14, No. 12, pp. 1675-1682. 1976.
5. Dahl, P.R., "Measurement of Solid Friction Parameters of Ball Bearings", Space And Missile Systems Organization Air Force System Command, Report No. SAMSO-TR-77-132.
6. La Technique Integrale Division of SKF, Chambery, France, Model PVCZ 12X1 R1 Roller Screw Through Use Representatives. The Prideaux Company, Rancho Palos Verdes, California.
7. Berthold, III, J.W. and Jacobs, S. F., "Ultraprecise Thermal Expansion Measurements of Seven Low-Expansion Materials", Applied Optics, Vol. 15, No. 10, pp. 2344-2347. 1976.
8. Simpson, J. A., "Use of a Microscope as a Non-Contacting Microdisplacement Measurement Device", RSI, Vol. 41, pp. 1378-1380. 1971.
9. Powell, J. A., "A Simple Two Fiber Optical Displacement Sensor", RSI, Vol. 45, No. 2, pp. 302-303. 1974.
10. KAMAM Measuring Systems, Colorado Springs, Colorado 80933. Inductive Detector, Model KD2300-.55U.
11. Usher, M. J., Buckner, I. W. and Burch, R. F., "A Miniature Wideband Horizontal-Component Feedback Seismometer, J. of Physics E:Scientific Instruments, Vol. 10, pp. 1253-1260. 1977.
12. Lion, K. S., "Non-linear Twin-T Network for Capacitive Transducers", RSI, Vol. 35, No. 3, pp. 353-356. 1964.
13. Peterson, O. and Anderson, W. E., "A Wide-Range High-Voltage Capacitance Bridge with One PPM Accuracy", IEEE Trans. Instr. and Measurement, Vol. IM-24, No. 4, pp. 336-344. 1975.
14. White, S. H. and Blessum, D. N., "High Precision Capacitance Bridge for Studying Lipid Bilayer Membranes", RSI, Vol. 46, No. 11, pp. 1462-1466. 1975.
15. Richards, J.C.S., "Proximity Gauges with High Resolution", J. of Physics E:Scientific Instruments, Vol. 9, pp. 639-646. 1976.
16. Jones, R. V. and Richards, J.C.S., "The design and Some Applications of Sensitive Capacitance Micrometers", J. of Physics E:Scientific Instruments, Vol. 6, pp. 589-600. 1973.
17. Berthold, III, W., etal, "Dimensional Stability of Fused Silica, Invar, and Several Ultralow Thermal Expansion Materials", Applied Optics, Vol. 15, No. 8, pp. 1898-1899. 1976.
18. Grimbleby, J. B. and Harding, D. W., "A New High-Performance Phase Sensitive Detector", J. of Physics E:Scientific Instruments, Vol. 4, pp. 941-944. 1971.

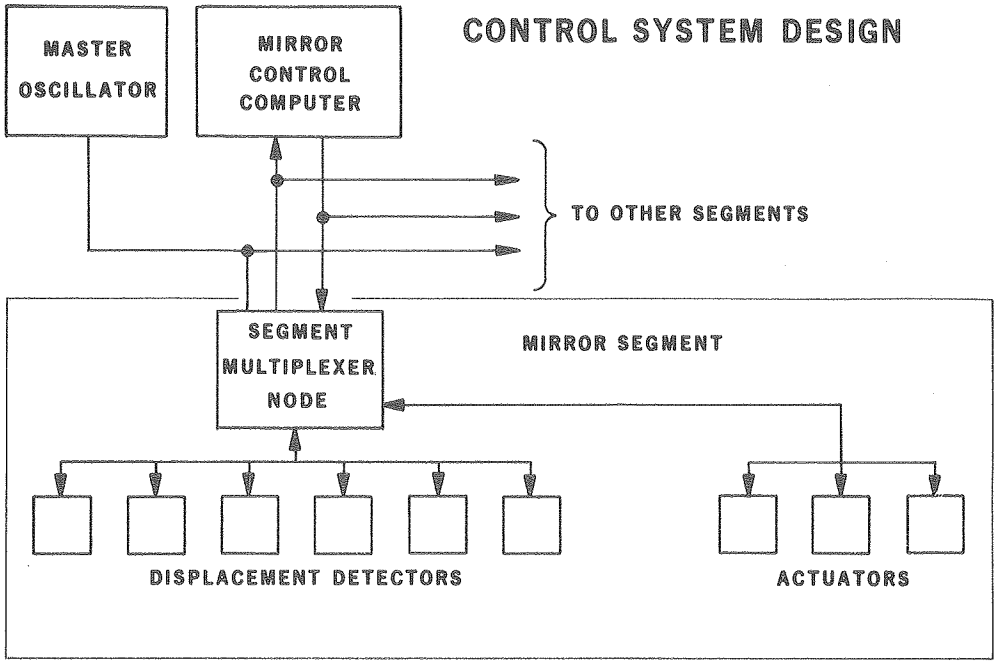

FIG. 1

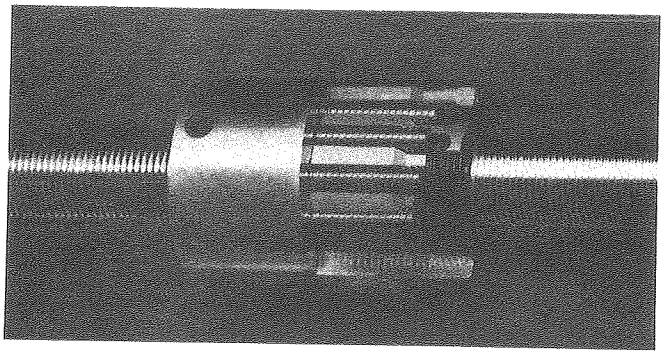

FIG. 2 RECIRCULATING PLANETARY ROLLER SCREW

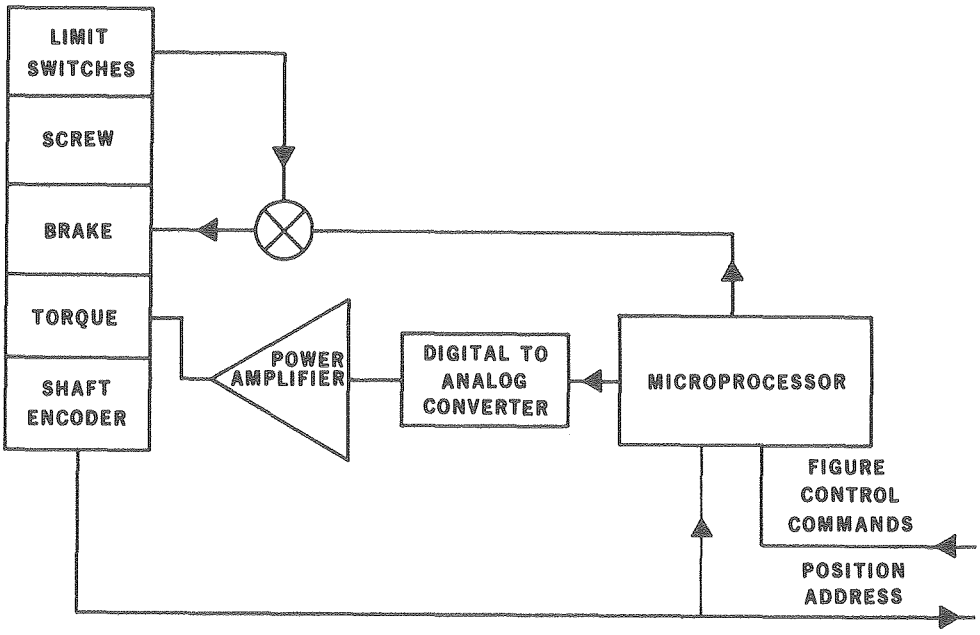

BLOCK DIAGRAM OF DISPLACEMENT ACTUATOR FIG. 3

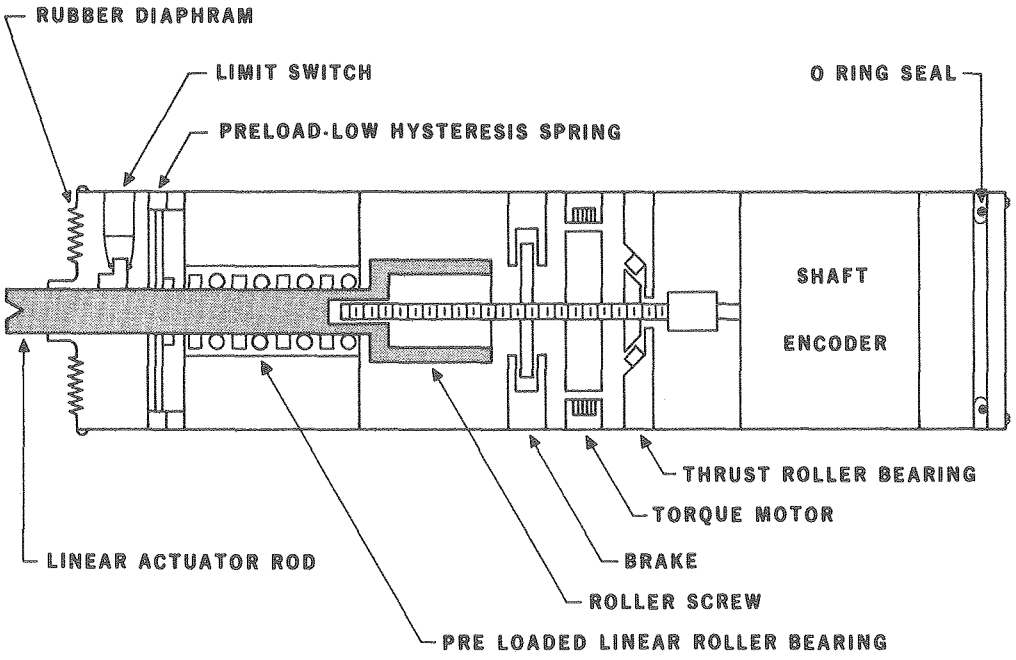

CROSS SECTION OF DISPLACEMENT ACTUATOR MECHANICAL LAYOUT FIG. 4

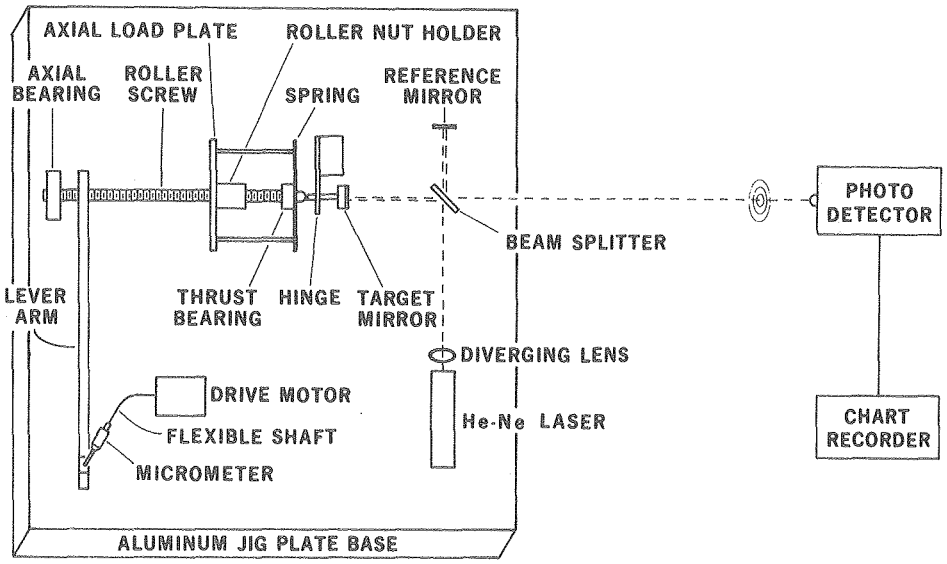

ROLLER SCREW TEST FIXTURE

FIG. 5

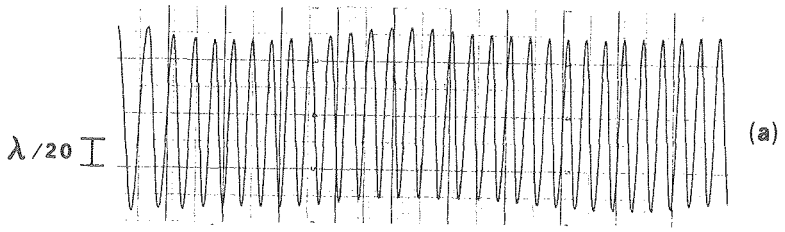

TEST FOR SMOOTHNESS AND MONOTONICITY

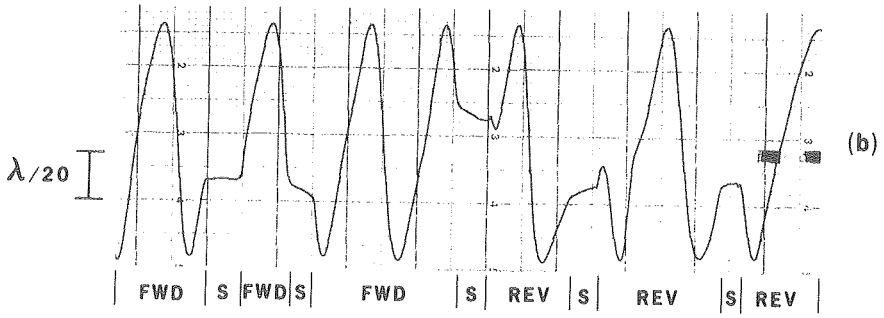

TEST FOR BACKLASH AND SLIPSTICK

INTERFEROMETER OUTPUT FOR ROLLER SCREW TESTS

FIG. 6

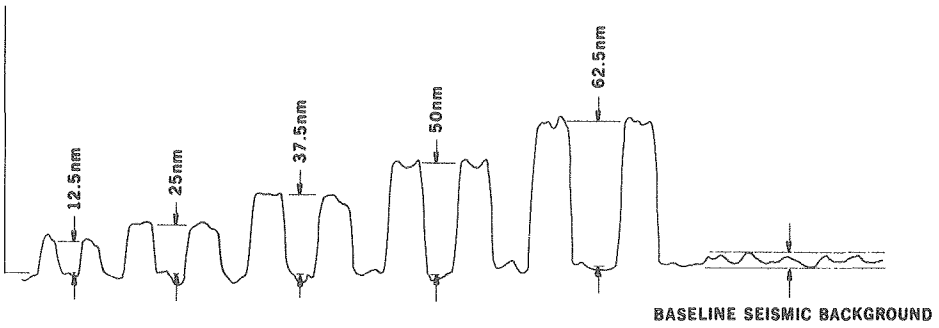

ROLLER SCREW DISPLACEMENT RESPONSE FOR INCREMENTAL STEP INPUT

FIG. 7

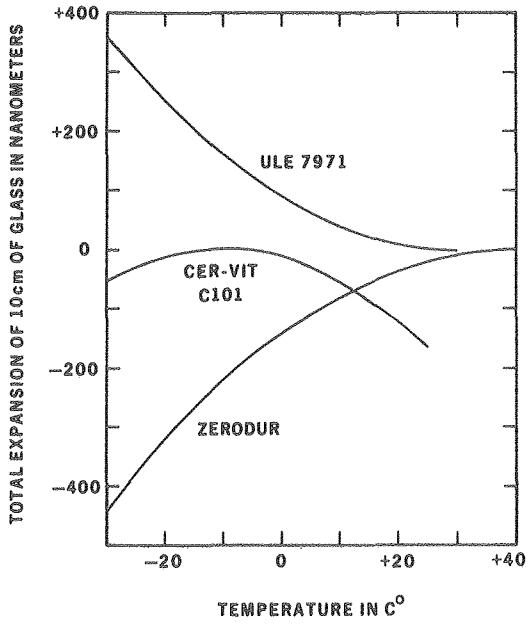

EXPANSION BEHAVIOR OF SEVERAL MIRROR GLASSES
WITH ZERO EXPANSION POINT AT α=0 TEMPERATURE

FIG. 8

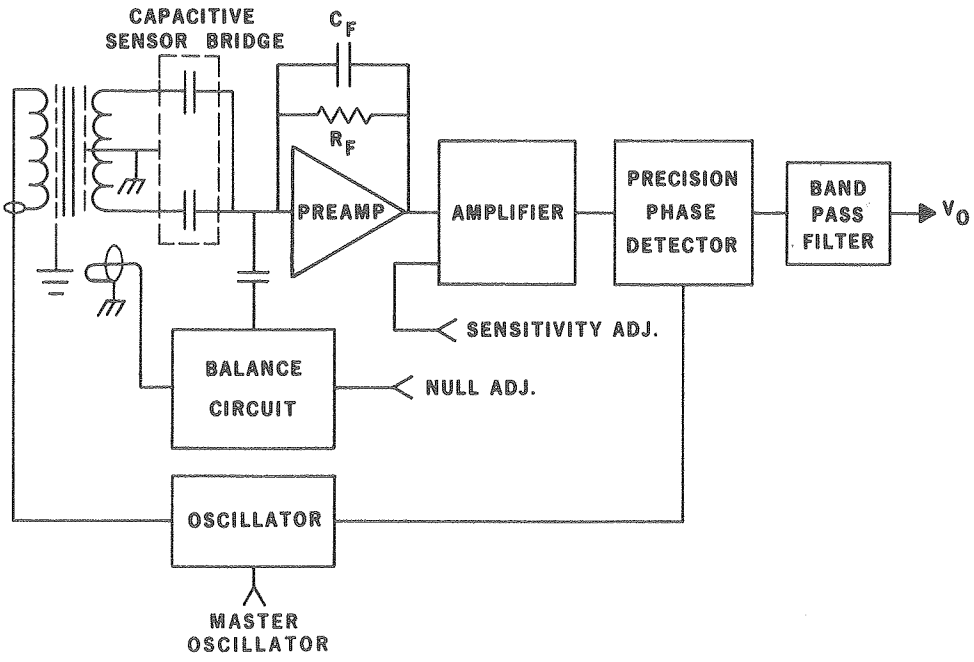

BLOCK DIAGRAM OF DISPLACEMENT DETECTOR

FIG. 9

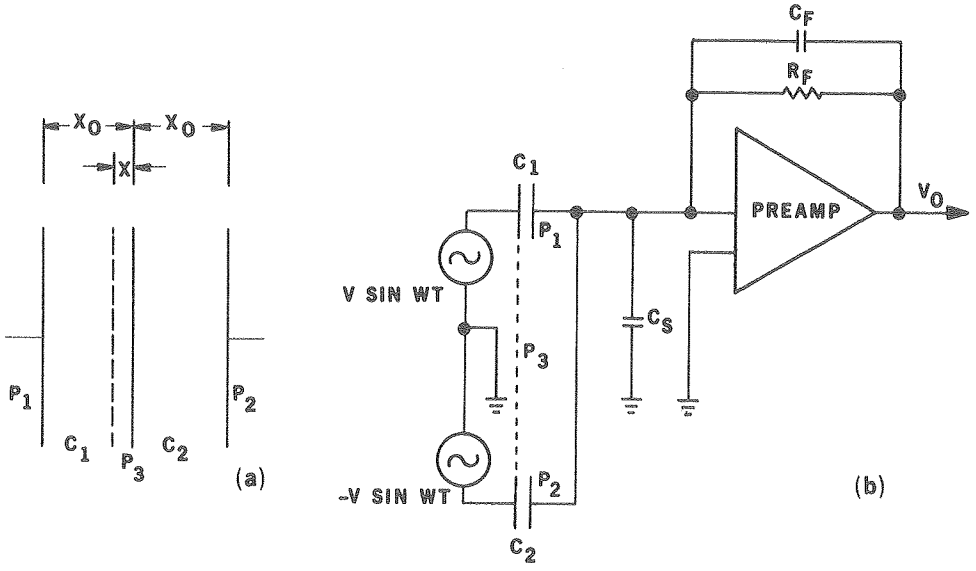

DISPLACEMENT
SENSOR MODEL

DISPLACEMENT SENSOR
AND PREAMP CIRCUIT

FIG. 10

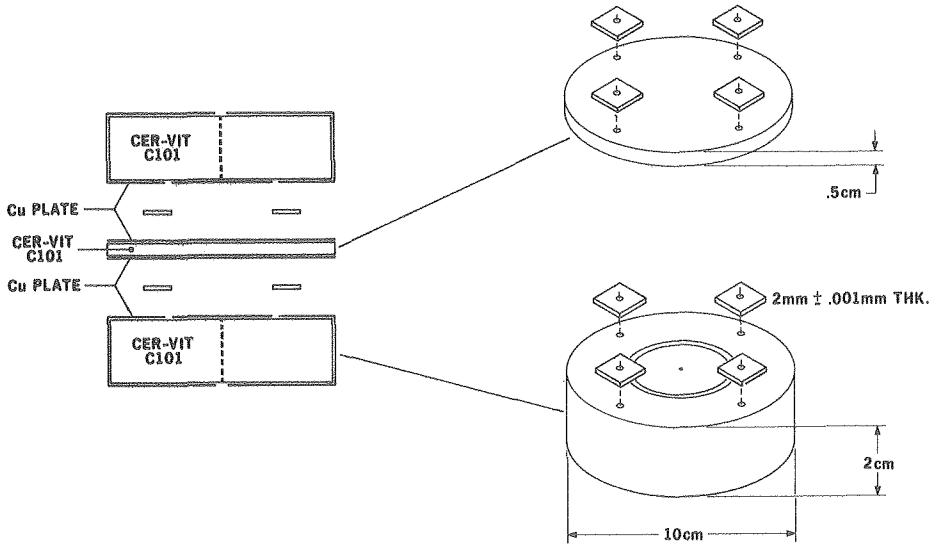

MECHANICAL CONFIGURATION FOR TEST DISPLACEMENT SENSOR

FIG.11

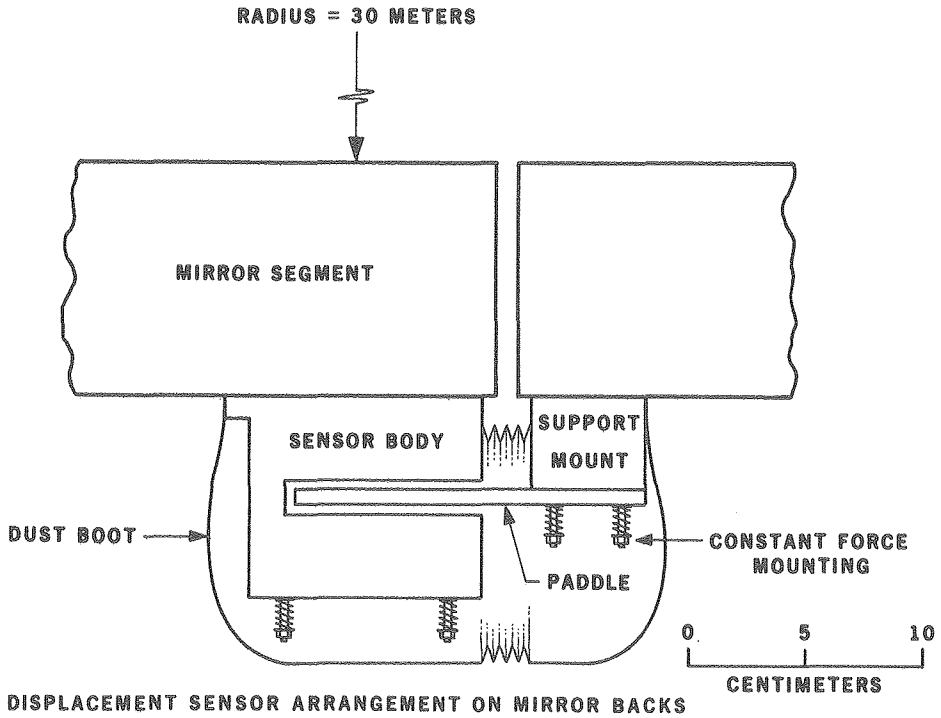

DISPLACEMENT SENSOR ARRANGEMENT ON MIRROR BACKS

FIG. 12

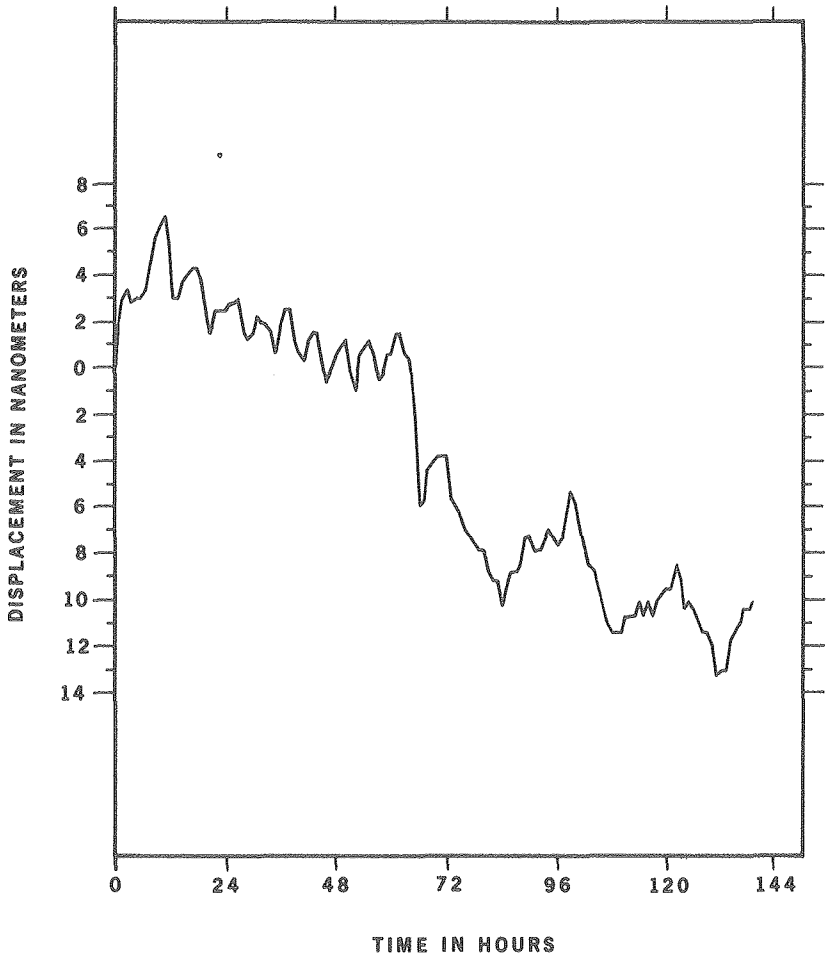

TEST OF DISPLACEMENT DETECTOR STABILITY WITH TIME

FIG. 13

TECHNICAL INFORMATION DEPARTMENT
LAWRENCE BERKELEY LABORATORY
UNIVERSITY OF CALIFORNIA
BERKELEY, CALIFORNIA 94720